

Improving the Rate-Loss Scaling in Polarization Entanglement Distribution using Single-Click Entanglement Swapping

Hikaru Shimizu^{1,*}, Joe Yoshimoto^{2,3}, Daiki Ichii¹, Junko Ishi-Hayase^{2,3}, Rikizo Ikuta^{4,5,†} and Masahiro Takeoka^{1,6‡}

¹*Department of Electronics and Electrical Engineering, Keio University, Kohoku-ku, Yokohama 223-8522, Japan*

²*School of Fundamental Science and Technology, Keio University, Kohoku-ku, Yokohama 223-8522, Japan*

³*Center for Spintronics Research Network, Keio University, Kohoku-ku, Yokohama 223-8522, Japan*

⁴*Graduate School of Engineering Science, Osaka University, Toyonaka, Osaka 560-8531, Japan*

⁵*Center for Quantum Information and Quantum Biology, Osaka University, Osaka 560-0043, Japan and*

⁶*National Institute of Information and Communications Technology (NICT), Koganei, Tokyo 184-8795, Japan*

(Dated: July 22, 2025)

Polarization entanglement is widely used in optical quantum information processing due to its compatibility with standard optical components. On the other hand, it is known that polarization entanglement is susceptible to the loss, more precisely, its transmission rate in a lossy channel is limited by the scaling of $O(\eta)$, where η is a transmittance of the channel. Here, we experimentally demonstrate that this rate-loss scaling limit can be overcome by a relatively simple protocol. This is possible by integrating the idea of the polarization-photon-number hybrid entanglement and the single-click entanglement swapping. We demonstrate square root improvement of the rate-loss scaling from the conventional approaches and achieve the fidelity of 0.843 for the distributed polarization entangled photon pairs. This improvement in the rate-loss scaling is equivalent to that achieved by 1-hop quantum repeater node. Our result paves a way to build a near-future quantum network and its applications.

Introduction.— Photonic polarization entanglement is a fundamental resource for various quantum information processing. The most notable feature is its compatibility with ordinary optical components. Due to its practicality and ease of use, polarization entanglement has been widely employed in various experiments: from fundamental science, e.g. quantum state tomography [1, 2] and Bell tests [3–5], to applications of quantum information such as entanglement-based quantum key distribution [6, 7], quantum sensing [8–10], quantum computing [11–15], as well as quantum network[16].

One of the practical issues of the polarization entanglement is the resistance to the channel loss. For an optical channel with transmittance η , the rate of distributing polarization entangled photons scales linearly with η . This is particularly a problem for long distance quantum communication [17, 18] since η decreases exponentially with the distance. It is also problematic even for short distance, to generate and apply multi-partite polarization entanglement [19, 20] since all multipartite photons must be successfully detected simultaneously. Experimentally, this is a critical problem since the required time to collect data easily goes to impractically long. In principle, quantum repeater [21–23] can overcome this problem and its technology is growing remarkably [24–29]. However, it is still not easy to leverage the rate-loss scaling advantage of quantum repeaters in real experiments.

In this paper, we experimentally demonstrate that the rate-loss scaling of distributing polarization entangled photon pairs through a lossy optical channel with transmittance η can be better than $O(\eta)$. This is achieved by combining the following two key ideas. First, we employ a single-click entanglement swapping, which utilizes the superposition of the vacuum and single-photon states.

This approach is known to surpass the scaling of direct transmission [30, 31] and can also be extended to the distribution of multi-partite entanglement [32, 33]. Several experimental demonstrations of this physical encoding have been reported [34, 35].

Second, we use the hybrid entanglement between polarization and photon-number qubits. This state is obtained by generating normal polarization or photon-number qubit entanglement and converting the degree of freedom [36] of one of the modes. An experimental study of hybrid entanglement generation has also been reported [37]. The basic idea of combining these techniques is as follows. We prepare hybrid entanglement sources at two end-uses, Alice and Bob, and then they send the photon-number superposition parts to lossy channels for the entanglement swapping. Then, it leverages the improved rate-loss scaling by the single-click entanglement swapping whereas the resulted state shared by Alice and Bob is a polarization entangled photon pair. Our result paves a way of expanding the practical usefulness of polarization entanglement in quantum network and multi-partite quantum information processings with currently feasible technologies.

Protocol overview.— The sources of the hybrid entanglement of polarization and photon-number qubits are prepared at both Alice’s and Bob’s end as shown in Fig. 1. The hybrid entanglement is generated by combining two optical quantum states. One is the two-mode polarization squeezed vacuum (TMSV) described as,

$$|\text{TMSV}\rangle \sim |0_H 0_V\rangle + \gamma |1_H 1_V\rangle + \mathcal{O}(\gamma^2), \quad (1)$$

for $|\gamma| \ll 1$, where $|0_{H(V)}\rangle$ is a vacuum state and $|1_{H(V)}\rangle$ is a single-photon state in the H(V)-polarized mode.

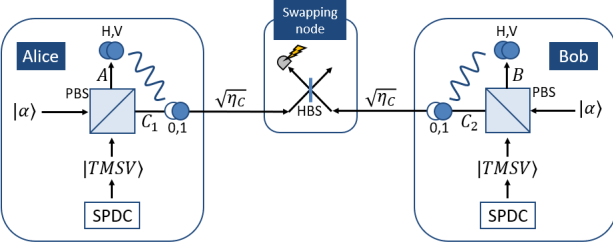


FIG. 1: Schematic image of the experiment. The Bell state measurement (BSM) in this protocol is based on the single-photon interference between the number-state photons coming from Alice and Bob. The single-photon detection at the BSM node heralds successful distribution of the polarization entangled photon pair.

TMSV can be generated by the spontaneous parametric down-conversion (SPDC) in a Type-II second-order nonlinear optical crystal. The other one is vertically polarized weak coherent light described as,

$$|\alpha\rangle \sim |0_V\rangle + \alpha |1_V\rangle + \mathcal{O}(\alpha^2), \quad (2)$$

for $|\alpha| \ll 1$. They are mixed by using a polarizing beam splitter (PBS). At Alice's side, by post-selecting the events where one or more photons exist in mode A, we obtain an unnormalized hybrid state in modes A and C_1 as

$$|\psi\rangle_{AC_1} = \alpha |V\rangle_A |0\rangle_{C_1} + \gamma |H\rangle_A |1\rangle_{C_1}, \quad (3)$$

where we omitted terms originating from components of the multiple photons in $|TMSV\rangle$ and $|\alpha\rangle$, which will be discussed later. Note that $|H(V)\rangle_A$ and $|n_V\rangle_{C_1}$ in Eq. (3) correspond to $|1_{H(V)}\rangle_A$ and $|n\rangle_{C_1}$, respectively, in the previous expressions. The same hybrid entanglement is also prepared in Bob's side, denoted as $|\psi\rangle_{BC_2}$.

The states in modes C_1 and C_2 are sent to the swapping node through optical channels with transmittance $\sqrt{\eta}$. The swapping is successful if single-photon detection occurs at one of the output of the BS in the swapping node. For the successful event, the total state is projected onto $\langle\Psi_{01}^+|_{C_1C_2} = (\langle 0|_{C_1} \langle 1|_{C_2} + \langle 1|_{C_1} \langle 0|_{C_2})/\sqrt{2}$, which acts as the BSM, and the resulting unnormalized state in A and B is given as,

$$\langle\Psi_{01}^+|_{C_1C_2} |\psi\rangle_{AC_1} |\psi\rangle_{BC_2} = \frac{\alpha\gamma\eta^{1/4}}{\sqrt{2}} |\Psi_{\text{pol}}^+\rangle_{AB}, \quad (4)$$

where,

$$|\Psi_{\text{pol}}^+\rangle_{AB} = \frac{1}{\sqrt{2}} (|H\rangle_A |V\rangle_B + |V\rangle_A |H\rangle_B), \quad (5)$$

is the polarization maximally entangled state. From the coefficient in Eq. (4), we find that the ideal success probability of our protocol is $|\alpha|^2|\gamma|^2\sqrt{\eta}/2$, i.e. it scales with

$\sqrt{\eta}$ for channel transmission while the rate of directly transmitting polarization entangled photons is proportional to η .

The factor $|\alpha|^2|\gamma|^2$ in the above success probability reflects the fact that the generated polarized photon pair consists of one photon from the TMSV and another photon from the coherent state. In practice, however, the higher order photons of the TMSV and the coherent state may also be included and contribute to degrade the fidelity to the ideal entanglement, where the leading terms of occurring these unwanted events are $|\gamma|^4\sqrt{\eta}$ and $|\alpha|^4|\gamma|^2\sqrt{\eta}$, respectively. To avoid them, therefore, $1 \gg |\alpha|^2 \gg |\gamma|^2$ must be satisfied. See Ref. [46] for more details of the protocols and the effect of the multiphotons from the TMSV and the coherent state.

Experimental setup.— Our experimental setup is shown in Fig. 2. For generating hybrid entangled states at Alice and Bob, we use a mode-locked fiber laser with the central wavelength of 1560 nm, the repetition rate of 1 GHz and the pulse width of 4.9 ps. After a portion of the laser light is used for the second harmonic generation (SHG) by a Type-0 periodically poled lithium niobate (PPLN) waveguide, the resulting SH light at 780 nm and the attenuated fundamental laser light at 1560 nm are distributed to Alice and Bob.

At Alice and Bob, the lights are separated by a dichroic mirror (DM). The SH light is used as a pump light to generate the TMSV in Eq. (1) at a Type-II PPLN waveguide. The V-polarized weak coherent light at 1560 nm written in Eq. (2) is mixed with the SPDC photons at a PBS after passing through a delay line and an optical attenuator (Att). This results in the hybrid entangled states $|\psi\rangle_{AC_1}$ at Alice's side, and $|\psi\rangle_{BC_2}$ at Bob's side. At each side, the mean photon number of the weak coherent light and excitation probability of SPDC are set to $|\alpha|^2 \sim 0.10$ and $|\gamma|^2 \sim 6.0 \times 10^{-3}$, respectively.

The photons at modes C_1 and C_2 are attenuated by variable neutral density (ND) filters, that act as the channel losses, and then sent to a swapping node through single-mode fibers. The photons are mixed at a fiber-based BS (FBS), and then they are measured by a photon detector connected to one of the output ports of the FBS. Heralded by this photon detection, the polarization-entangled state in modes A and B is shared between Alice and Bob. To maximize the fidelity of the entanglement swapping, an optical delay line is inserted into the fiber for synchronizing the arrival time of the wave packets. In addition, a fiber stretcher is installed for phase stabilization, which is stabilized by the reference light centered at 1558 nm, traveling along two separate paths originating from Alice and Bob. The reference light is removed by a DWDM at one of the output ports of the FBS where the photon detection is performed. At the other output port, the reference light is detected by a photodiode, and the resulting signal is used for PID feedback to stabilize the optical path length.

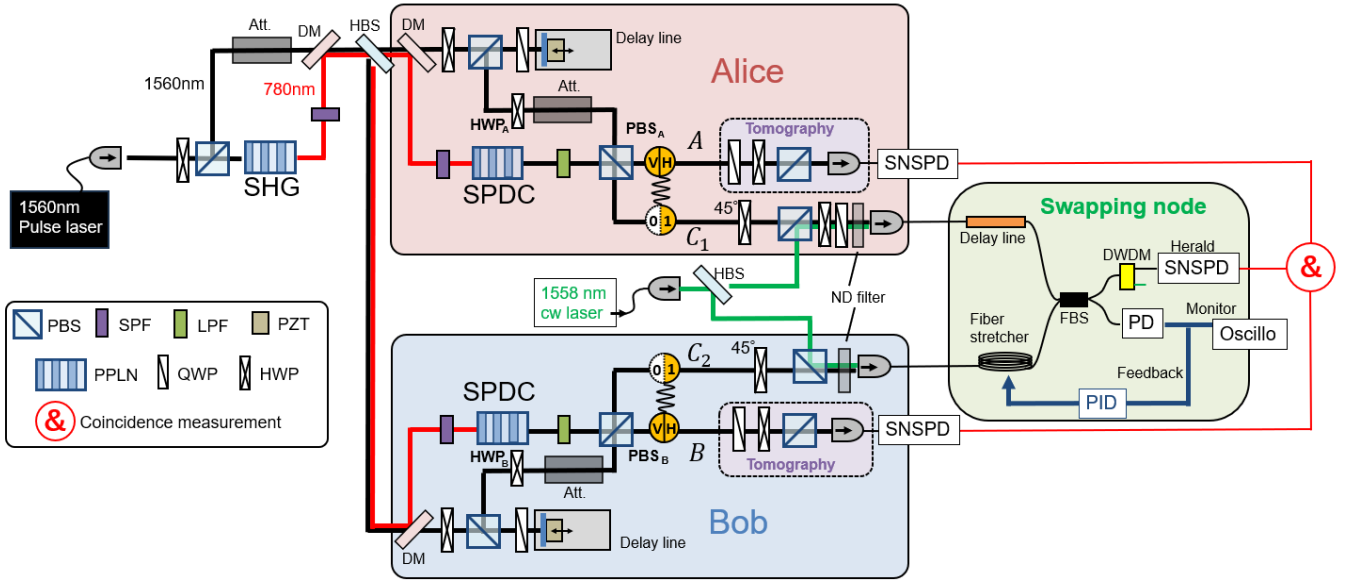


FIG. 2: Experimental setup. PBS: polarizing beam splitter, SPF: short-pass filter, DM: dichroic mirror, HBS: half beam splitter, QWP: quarter-wave plate, HWP: half-wave plate, PPLN: periodically poled lithium niobate, LPF: long-pass filter, ND filter: neutral density filter, FBS: fiber beam splitter, DWDM: dense wavelength division multiplexer, and PD: photodiode.

Each of the two photons at modes A and B is measured by a photon detector equipped with a quarter-wave plate (QWP), a half-wave plate (HWP), and a PBS for quantum state tomography [2]. In all experiments, we use superconducting nanowire single-photon detectors (SNSPDs) with their quantum efficiencies of $\sim 80\%$. The three photons measured by the SNSPDs are spectrally filtered using fiber-based bandpass filters with the bandwidths of 0.4 nm.

Evaluation of the hybrid entanglement.— The quality of the hybrid entanglement source is mainly determined by the mode overlap between the SPDC photons and the weak coherent light. For Alice’s source, this is evaluated by turning off Bob’s pump and rotating HWP_A such that the portion of the coherent light, $|0_V\rangle_A + \alpha|1_V\rangle_A$, is in the H-polarization, $|0_H\rangle_{C_1} + \beta|1_H\rangle_{C_1}$. The SPDC photons and the weak coherent state are directly interfered at PBS_A. Then conditioned on the photon detection at mode C₁, the state in mode A before the HWP and the PBS (in the box of “Tomography”) is $|\phi\rangle_A = |\alpha||\beta||V\rangle_A + e^{i\theta}|\gamma||H\rangle_A$ if they are perfectly overlapped, where $\theta = \varphi_\gamma - \varphi_\alpha - \varphi_\beta$ ($\varphi_\gamma, \varphi_\alpha, \varphi_\beta$ are the phase of γ, α and β). Then the visibility of the first and second terms of $|\phi\rangle_A$ is observed by projecting them onto the diagonal polarization by the HWP and the PBS. In this setting, with $|\alpha||\beta| = |\gamma|$, the coincidence probability of modes A and C₁ directly reflects the overlap of the SPDC photons and the weak coherent light. This also works for Bob’s source. Figure 3 shows the experimental results of the oscillation of the coincidence probabilities between A and C₁ at Alice and B and C₂ at Bob. Note

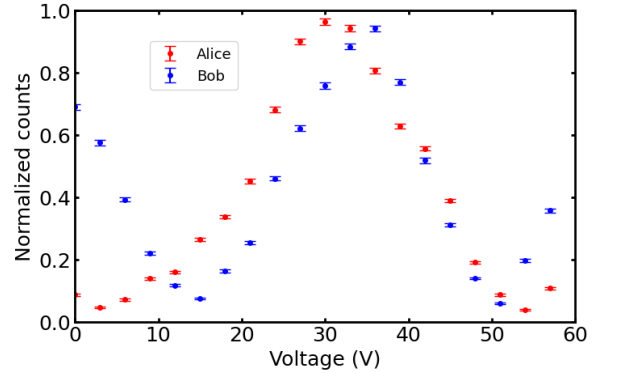


FIG. 3: The observed coincidence counts between A (B) and C₁ (C₂) at Alice (Bob), plotted in red (blue). The horizontal axis represents the voltage applied to the PZT mounted on the free-space delay line, which corresponds to phase θ .

that the coincident counts from the multi-photon terms of the SPDC and coherent states are pre-measured and removed from the figure. Then the visibilities, i.e. the mode overlaps, are estimated as $M_A = 0.924 \pm 0.004$ and $M_B = 0.881 \pm 0.006$, respectively. See Ref. [46] for the details of this evaluation.

Entanglement swapping.— First, we fixed the channel transmittance η_C in modes C₁ and C₂ to be 0.066 and performed the single-click entanglement swapping. For the successful events, we reconstructed the density matrix of the polarization entangled state by the two-

qubit quantum state tomography. The channel transmittance η_C includes all losses in modes C_1 and C_2 except for the detection efficiency η_D of the detectors. η_D includes the efficiency of the bandpass filter followed by the SNSPD and is around 0.12 for all detectors. The channel transmittances for the local channel at Alice's and Bob's sides, are $\eta_{LC} \sim 0.2$. The reconstructed density matrix ρ is shown in Fig. 4. The fidelity to the ideal polarization entangled state, defined as $\langle \psi_{\text{pol}}^+ | \rho | \psi_{\text{pol}}^+ \rangle$, is 0.843 ± 0.074 , which shows the successful entanglement distribution between Alice and Bob. From the theoretical model including the mode mismatches of the hybrid entangled states, the fidelity is estimated to be $(1 + M_A M_B)/2 = 0.907 \pm 0.003$, which fits with the experimental result and shows that the main imperfection comes from the mode mismatch in the hybrid sources.

Next, we performed a similar experiment under various channel losses in paths C_1 and C_2 . Figure 5 plots the distribution rates (coincidence count rates) as a function of the channel loss. The number at the squared plot is the fidelity whereas the numbers at the circled plots are the lower bound of the fidelity. The lower bound of the fidelity [38, 39] is estimated as $F_{\text{LB}} = (-V_{ZZ} + V_{XX})/2$, instead of performing full tomography, where the visibilities $V_{ZZ} = \langle Z_A Z_B \rangle$ and $V_{XX} = \langle X_A X_B \rangle$ are determined based on the Pauli operators $Z = |H\rangle\langle H| - |V\rangle\langle V|$ and $X = |+\rangle\langle +| - |-\rangle\langle -|$, where $|\pm\rangle = (|H\rangle \pm |V\rangle)/\sqrt{2}$. The plots clearly show that the rate-loss scaling proportional to $\sqrt{\eta}$.

The distribution rate of our protocol R_{hybrid} is estimated to be

$$R_{\text{hybrid}} = \frac{1}{2} |\alpha|^2 |\gamma|^2 \sqrt{\eta_C} \times \eta_{LC}^2 \times \eta_D^3 \times f_{\text{rep}}, \quad (6)$$

where $f_{\text{rep}} = 1 \text{ GHz}$ is the repetition rate and the other parameters in the experiment are $|\alpha|^2 \sim 0.10$, $|\gamma|^2 \sim 6.0 \times 10^{-3}$, $\eta_{LC} \sim 0.20$, and $\eta_D \sim 0.12$. This is indicated by the red solid line in Fig. 5, which shows

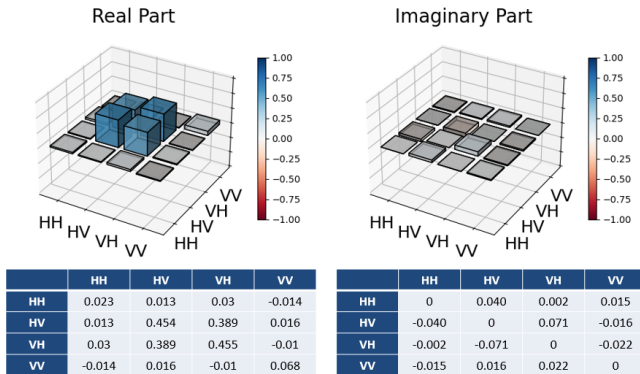


FIG. 4: Reconstructed density matrix of the distributed state. The measurement time for each polarization setting was 15 s. The distribution rate was 6.6 Hz.

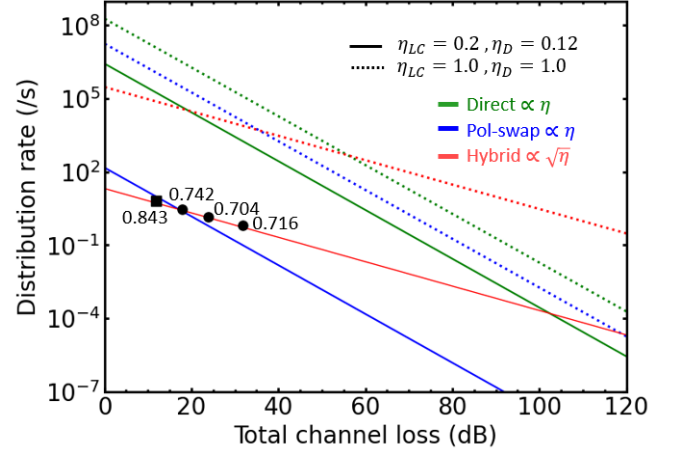


FIG. 5: Rate-loss scaling. Green, blue, and red lines show direct transmission protocol, protocol based on two-photon interference, and our protocol (hybrid), respectively. Black plots are experimental data. The numbers near the plots indicate the fidelity for the square plot and the lower bound of the fidelity for the circle plots. Including error bars, the values are 0.742 ± 0.048 , 0.704 ± 0.070 , and 0.716 ± 0.058 , respectively, from left to right. The solid lines use $\eta_{LC} = 0.2$ and $\eta_D = 0.12$, and dotted ones use $\eta_{LC} = \eta_D = 1.0$.

good agreement with the experimental data. As a reference, the ideal performance of this protocol without unwanted optical losses in the system, calculated using $\eta_{LC} = \eta_D = 1.0$, is shown as a red dotted line.

In Fig. 5, the result is compared with the standard entanglement swapping using two-photon interference [40] between polarization-entangled photon pairs [41–44]. Its rate is given by $R_{\text{pol-swap}} = \frac{1}{2} R_{\text{gen}}^2 \eta_C \eta_D^4 \eta_{LC}^2 f_{\text{rep}}$, where R_{gen} is the photon-pair generation probability for the SPDC which directly corresponds to $|\alpha|^2$ and f_{rep} is the repetition rate of the pump pulse. For fair comparison, these parameters are chosen to be the same as that of our experiment. This is indicated by the blue solid line in the figure. Our result is outperforming the standard entanglement swapping as well as showing the square-root advantage of the rate-loss scaling. We also made a comparison with the direct transmission of the polarization-entangled photon pairs. Its rate is given by $R_{\text{direct}} = R_{\text{gen}} \eta_C \eta_D^2 f_{\text{rep}}$, which is still below this line, they cross at the high-loss regime ($\sim 105 \text{ dB}$). Moreover, in principle, the performance of our protocol can be largely increased by improving the local channel transmittance and the detection efficiency. The rates with $\eta_{LC} = \eta_D = 1$ are compared by the dotted lines, where we observed that the crossover of our protocol and the other protocols occur at significantly lower loss regime.

Bell test.— Finally, we performed the CHSH-type Bell test [45] on the distributed polarization-entangled photons as a demonstration of quantum network application. In this experiment, we removed ND filters in front of the fiber collimators. Alice’s measurement bases are $Q : \{|H\rangle, |V\rangle\}$ and $R : \{|+\rangle, |-\rangle\}$, and Bob’s are $S : \{|\theta\rangle, |\theta + 90^\circ\rangle\}$ and $T : \{|-\theta\rangle, |-\theta + 90^\circ\rangle\}$, where $|\theta\rangle = \cos\theta|H\rangle + \sin\theta|V\rangle$. For each measurement basis, we assign +1 to the first basis vector and -1 to the second. The CHSH parameter S is determined by

$$S = |\langle QS \rangle + \langle QT \rangle + \langle RS \rangle - \langle RT \rangle|. \quad (7)$$

From the simulation of the Bell test on the reconstructed density matrix ρ in Fig. 4, the S parameter is expected to reach its maximum value of 2.313 at $\theta = -21.5^\circ$. Based on this simulation result, we carried out the Bell test in an actual experiment at the angle. The observed value of the S parameter was 2.302 ± 0.066 , which is in good agreement with the simulation result. The experimental value clearly violates the upper bound of 2 predicted by any local hidden variable theory, by approximately 5 standard deviations.

Discussion.— Our result can be extended to the multipartite entanglement distribution scenario. In Refs. [32, 33], protocols for efficiently distributing photon-number based multipartite entangled states, such as W, Dicke, and GHZ states, are proposed. Combining these with our hybrid approach enables to distributed polarization based multipartite entangled states with better rate-loss scaling. The advantage compared to the direct transmission is more prominent than that of the bipartite case [46]. Especially, we find that an application of our hybrid approach to the efficient GHZ-state distribution scenario can remedy the problem of multi-photon effects observed in Ref. [33] by the entanglement distillation-like effect. See Ref. [46] for its details.

In conclusion, we demonstrate a protocol of efficiently distributing polarization entanglement by using the hybrid entanglement sources and the single-click entanglement swapping. The distributed state shows high fidelity to the ideal polarization Bell state and we experimentally observe the square-root improvement of the rate-loss scaling from the conventional protocols. In addition, our technique is directly applicable to the protocol of efficiently distributing multipartite polarization entangled states. We are sure this study will accelerate research into large-scale quantum network applications.

Acknowledgements.— R.I. and M.T. acknowledge the members of the Quantum Internet Task Force for the comprehensive and interdisciplinary discussions on the quantum internet. This work was supported by JST CREST, JPMJCR24A5; MEXT Q-LEAP, JPMXS0118067395; Center for Spintronics Research Network (CSRN), Keio University; NEXT Leading Initiative for Excellent Young Researchers; Program for the Advancement of Next Generation Research Projects, Keio

University; JST CRONOS, JPMJCS24N6; JST ASPIRE, JPMJAP2427; JST Moonshot R&D, JPMJMS2061, JPMJMS226C, JPMJMS2066; R & D of ICT Priority Technology Project JPMI00316; and FOREST Program, JST JPMJFR222V.

* shimihika2357@keio.jp

† ikuta.rikizo.es@osaka-u.ac.jp

‡ takeoka@elec.keio.ac.jp

- [1] A. G. White, D. F. V. James, P. H. Eberhard, and P. G. Kwiat, Nonmaximally Entangled States: Production, Characterization, and Utilization, *Phys. Rev. Lett.* **83**, 3103 (1999).
- [2] D. F. V. James, P. G. Kwiat, W. J. Munro, and A. G. White, Measurement of qubits, *Phys. Rev. A* **64**, 052312 (2001).
- [3] M. Giustina, M. A. M. Versteegh, S. Wengerowsky, J. Handsteiner, A. Hochrainer, K. Phelan, F. Steinlechner, J. Kofler, J. Larsson, C. Abellán, W. Amaya, V. Pruneri, M. W. Mitchell, J. and Beyer, T. Gerrits, A. E. Lita, L. K. Shalm, S. W. Nam, T. Scheidl, R. Ursin, B. Wittmann, and A. Zeilinger, Significant-Loophole-Free Test of Bell’s Theorem with Entangled Photons, *Phys. Rev. Lett.* **115**, 250401 (2015).
- [4] Y. Tsujimoto, K. Wakui, M. Fujiwara, K. Hayasaka, S. Miki, H. Terai, M. Sasaki, and M. Takeoka, Optimal conditions for the Bell test using spontaneous parametric down-conversion sources, *Phys. Rev. A* **98**, 063842 (2018).
- [5] W. -Z. Liu, Y. -Z. Zhang, Y. -Z. Zhen, M. -H. Li, Y. Liu, J. Fan, F. Xu, Q. Zhang, and J. -W. Pan, Toward a Photonic Demonstration of Device-Independent Quantum Key Distribution, *Phys. Rev. Lett.* **129**, 050502 (2022).
- [6] Y. Shi, S. M. Thar, H. S. Poh, J. A. Grieve, C. Kurtsiefer, and A. Ling, *Appl. Phys. Lett.* **117**, 124002 (2020).
- [7] J. Yin, Y. -H. Li, S. -K. Liao, M. Yang, Y. Cao, L. Zhang, J. -G. Ren, W. -Q. Cai, W. -Y. Liu, S. -L. Li, R. Shu, Y. -M. Huang, L. Deng, L. Li, Q. Zhang, N. -L. Liu, Y. -A. Chen, C. -Y. Lu, X. -B. Wang, F. Xu, J. -Y. Wang, C. -Z. Peng, A. K. Ekert and J. -W. Pan, Entanglement-based secure quantum cryptography over 1,120 kilometres, *Nature* **582**, 501–505 (2020).
- [8] D. -H. Kim, S. Hong, Y. -S. Kim, Y. Kim, S. -W. Lee, R. C. Pooser, K. Oh, S. -Y. Lee, C. Lee, and H. -T. Lim, Distributed quantum sensing of multiple phases with fewer photons. *Nat Commun* **15**, 266 (2024).
- [9] S. -R. Zhao, Y. -Z. Zhang, W. -Z. Liu, J. -Y. Guan, W. Zhang, C. -L. Li, B. Bai, M. -H. Li, Y. Liu, L. You, J. Zhang, J. Fan, F. Xu, Q. Zhang, and J. -W. Pan, Field Demonstration of Distributed Quantum Sensing without Post-Selection, *Phys. Rev. X* **11**, 031009 (2021).
- [10] L. -Z. Liu, Y. -Z. Zhang, Z. -D. Li, R. Zhang, X. -F. Yin, Y. -Y. Fei, L. Li, N. -L. Liu, F. Xu, Y. -A. Chen, and J. -W. Pan, Distributed quantum phase estimation with entangled photons. *Nat. Photonics* **15**, 137–142 (2021).
- [11] S. Gasparoni, J. -W. Pan, P. Walther, T. Rudolph, and A. Zeilinger, Realization of a Photonic Controlled-NOT Gate Sufficient for Quantum Computation, *Phys. Rev. Lett.* **93**, 020504 (2004).
- [12] P. Walther, K. J. Resch, T. Rudolph, E. Schenck, H. Weinfurter, V. Vedral, M. Aspelmeyer, and A. Zeilinger,

- Experimental one-way quantum computing, *Nature* **434**, 169–176 (2005).
- [13] K. Chen, C. -M. Li, Q. Zhang, Y. -A. Chen, A. Goebel, S. Chen, A. Mair, and J. -W. Pan, Experimental Realization of One-Way Quantum Computing with Two-Photon Four-Qubit Cluster States, *Phys. Rev. Lett.* **99**, 120503 (2007).
- [14] Y. Tokunaga, S. Kuwashiro, T. Yamamoto, M. Koashi, and N. Imoto, Generation of High-Fidelity Four-Photon Cluster State and Quantum-Domain Demonstration of One-Way Quantum Computing, *Phys. Rev. Lett.* **100**, 210501 (2008).
- [15] A. Crespi, R. Ramponi, R. Osellame, L. Sansoni, I. Bongioanni, F. Sciarrino, G. Vallone, and P. Mataloni, Integrated photonic quantum gates for polarization qubits. *Nat Commun* **2**, 566 (2011).
- [16] A. N. Craddock, A. Lazenby, G. B. Portmann, R. Sekelsky, M. Flament, and M. Namazi, Automated Distribution of Polarization-Entangled Photons Using Deployed New York City Fibers, *PRX Quantum* **5**, 030330 (2024).
- [17] S. Wengerowsky, S. K. Joshi, F. Steinlechner, J. R. Zichi, B. Liu, T. Scheidl, S. M. Dobrovolskiy, R. van der Molen, J. W. N. Los, V. Zwiller, M. A. M. Versteegh, A. Mura, D. Calonico, M. Inguscio, A. Zeilinger, A. Xuereb, and R. Ursin, Passively stable distribution of polarisation entanglement over 192 km of deployed optical fibre. *npj Quantum Inf* **6**, 5 (2020).
- [18] S. P. Neumann, A. Buchner, L. Bulla, M. Bohmann, and R. Ursin, Continuous entanglement distribution over a transnational 248 km fiber link. *Nat Commun* **13**, 6134 (2022).
- [19] W. McCutcheon, A. Pappa, B. A. Bell, A. McMillan, A. Chailloux, T. Lawson, M. Mafu, D. Markham, E. Diamanti, I. Kerenidis, J. G. Rarity, and M. S. Tame, Experimental verification of multipartite entanglement in quantum networks, *Nat Commun* **7**, 13251 (2016).
- [20] M. Proietti, J. Ho, F. Grasselli, P. Barrow, M. Malik, and A. Fedrizzi, Experimental quantum conference key agreement, *Sci. Adv.* **7**, eabe0395(2021).
- [21] H.-J. Briegel, W. Dür, J. I. Cirac, and P. Zoller, Quantum Repeaters: The Role of Imperfect Local Operations in Quantum Communication, *Phys. Rev. Lett.* **81**, 5932 (1998).
- [22] N. Sangouard, C. Simon, H. de Riedmatten, and N. Gisin, Quantum repeaters based on atomic ensembles and linear optics, *Phys. Rev. Lett.* **81**, 5932 (2011).
- [23] K. Azuma, S. E. Economou, D. Elkouss, P. Hilaire, L. Jiang, H. -K. Lo, and I. Tzitrin, Quantum repeaters: From quantum networks to the quantum internet, *Rev. Mod. Phys.* **95**, 045006 (2023).
- [24] Y. Hasegawa, R. Ikuta, N. Matsuda, K. Tamaki, H. Lo, T. Yamamoto, K. Azuma, and N. Imoto, Experimental Time-reversed Adaptive Bell Measurement towards All-photonic Quantum Repeaters, *Nat Commun* **10**, 378 (2019).
- [25] ZD. Li, R. Zhang, XF. Yin et al., Experimental quantum repeater without quantum memory, *Nat. Photon.* **13**, 644–648 (2019).
- [26] V. Krutyanskiy, M. Canteri, M. Meraner, J. Bate, V. Krucmarsky, J. Schupp, N. Sangouard, and B. P. Lanyon, Telecom-Wavelength Quantum Repeater Node Based on a Trapped-Ion Processor, *Phys. Rev. Lett.* **130**, 213601 (2023).
- [27] JL. Liu, XY. Luo, Y. Yu et al., Creation of memory-memory entanglement in a metropolitan quantum network, *Nature* **629**, 579–585 (2024).
- [28] A. J. Stolk et al., Metropolitan-scale heralded entanglement of solid-state qubits, *Sci. Adv.* **10**, eadp6442 (2024).
- [29] J. Hänni, A. E. Rodríguez-Moldes, F. Appas, S. Wengerowsky, D. Lago-Rivera, M. Teller, S. Grandi, and H. de Riedmatten, Heralded entanglement of on-demand spin-wave solid-state quantum memories for multiplexed quantum network links, arXiv:2501.04131.
- [30] E. T. Campbell and S. C. Benjamin, Measurement-Based Entanglement under Conditions of Extreme Photon Loss, *Phys. Rev. Lett.* **101**, 130502 (2008).
- [31] M. Lucamarini, Z. L. Yuan, J. F. Dynes, and A. J. Shields, Overcoming the rate-distance limit of quantum key distribution without quantum repeaters, *Nature* **557**, 400–403 (2018).
- [32] W. Roga, R. Ikuta, T. Horikiri, and M. Takeoka, Efficient Dicke-state distribution in a network of lossy channels, *Phys. Rev. A* **108**, 012612 (2023).
- [33] H. Shimizu, W. Roga, D. Elkouss, and M. Takeoka, Simple loss-tolerant protocol for Greenberger-Horne-Zeilinger-state distribution in a quantum network, *Phys. Rev. A* **111**, 022624 (2025).
- [34] P. Caspar, E. Verbanis, E. Oudot, N. Maring, F. Samara, M. Caloz, M. Perrenoud, P. Sekatski, A. Martin, N. Sangouard, H. Zbinden, and R. T. Thew, Heralded Distribution of Single-Photon Path Entanglement, *Phys. Rev. Lett.* **125**, 110506 (2020).
- [35] W. Zo, B. Bilash, D. Lee, Y. Kim, H. -T. Lim, K. Oh, S. M. Assad, and Y. -S. Kim, Entanglement swapping via lossy channels using photon-number-encoded states, *Phys. Rev. A* **110**, 052603 (2024).
- [36] J. Fiurášek, Interconversion between single-rail and dual-rail photonic qubits, *Phys. Rev. A* **95**, 033802 (2017).
- [37] D. Drahi, D. V. Sychev, K. K. Pirov, E. A. Sazhina, V. A. Novikov, I. A. Walmsley, and A. I. Lvovsky, Entangled resource for interfacing single- and dual-rail optical qubits, *Quantum* **5**, 416 (2021).
- [38] K. Nagata, M. Koashi, N. Imoto, Observables suitable for restricting the fidelity to multipartite maximally entangled states, *Phys. Rev. A* **65**, 042314 (2002).
- [39] R. Ikuta, Y. Ono, T. Tashima, T. Yamamoto, M. Koashi, N. Imoto, Efficient decoherence-free entanglement distribution over lossy quantum channels, *Phys. Rev. Lett.* **106**, 110503 (2011).
- [40] C. K. Hong, Z. Y. Ou, and L. Mandel, Measurement of subpicosecond time intervals between two photons by interference, *Phys. Rev. Lett.* **59**, 2044 (1987).
- [41] R. -B. Jin, M. Takeoka, U. Takagi, R. Shimizu, and M. Sasaki, Highly efficient entanglement swapping and teleportation at telecom wavelength, *Sci Rep* **5**, 9333 (2015).
- [42] Y. Tsujimoto, M. Tanaka, N. Iwasaki, R. Ikuta, S. Miki, T. Yamashita, H. Terai, T. Yamamoto, M. Koashi, and N. Imoto, High-fidelity entanglement swapping and generation of three-qubit GHZ state using asynchronous telecom photon pair sources. *Sci Rep* **8**, 1446 (2018).
- [43] X. -H. Zhan, Z. -Q. Zhong, S. Wang, Z. -Q. Yin, W. Chen, D. -Y. He, G. -C. Guo, and Z. -F. Han, Measurement-Device-Independent Quantum Key Distribution with Practical Spontaneous Parametric Down-Conversion Sources, *Phys. Rev. Applied* **20**, 034069 (2023).
- [44] X. -H. Zhan, Z. -Q. Zhong, J. -Y. Ma, S. Wang, Z. -Q. Yin, W. Chen, D. -Y. He, G. -C. Guo, and Z. -F. Han, Experimental demonstration of long distance quantum

communication with independent heralded single photon sources. *npj Quantum Inf* **11**, 73 (2025).

- [45] J. F. Clauser, M. A. Horne, A. Shimony, R. A. Holt, Proposed Experiment to Test Local Hidden-Variable Theories, *Phys. Rev. Lett.* **23**, 880 (1969).
- [46] Supplemental material.

Supplemental Material: Improving the Rate-Loss Scaling in Polarization Entanglement Distribution using Single-Click Entanglement Swapping

EXPLICIT DESCRIPTION OF THE EXPERIMENT

Two-mode squeezed vacuum (TMSV) state from the type-II spontaneous parametric down conversion (SPDC) sources is,

$$|\text{TMSV}\rangle = \sqrt{1 - \gamma^2} \sum_{n=0}^{\infty} \gamma^n |n_H n_V\rangle. \quad (1)$$

The weak coherent state that each user prepares in vertically polarized mode is

$$|\alpha\rangle = e^{-\frac{|\alpha|^2}{2}} \sum_{n=0}^{\infty} \frac{\alpha^n}{\sqrt{n!}} |n_V\rangle. \quad (2)$$

When these two states are input into a polarizing beam splitter from different ports (see Fig. S1(a)), the output is,

$$\begin{aligned} |\psi\rangle_{AC_1} &= |\alpha_V\rangle_A \otimes |\text{TMSV}\rangle_{AC_1} \\ &= e^{-\frac{|\alpha|^2}{2}} \sqrt{1 - \gamma^2} [|0_V\rangle_A |0_H 0_V\rangle_{AC_1} + \alpha |1_V\rangle_A |0_H 0_V\rangle_{AC_1} + \gamma |0_V\rangle_A |1_H 1_V\rangle_{AC_1} \\ &\quad + \frac{\alpha^2}{\sqrt{2}} |2_V\rangle_A |0_H 0_V\rangle_{AC_1} + \gamma^2 |0_V\rangle_A |2_H 2_V\rangle_{AC_1} + \alpha\gamma |1_V\rangle_A |1_H 1_V\rangle_{AC_1} + \dots]. \end{aligned} \quad (3)$$

Hereafter, we omit the normalization term $e^{-\frac{|\alpha|^2}{2}} \sqrt{1 - \gamma^2}$, as it is close to 1. This is the initial state generated

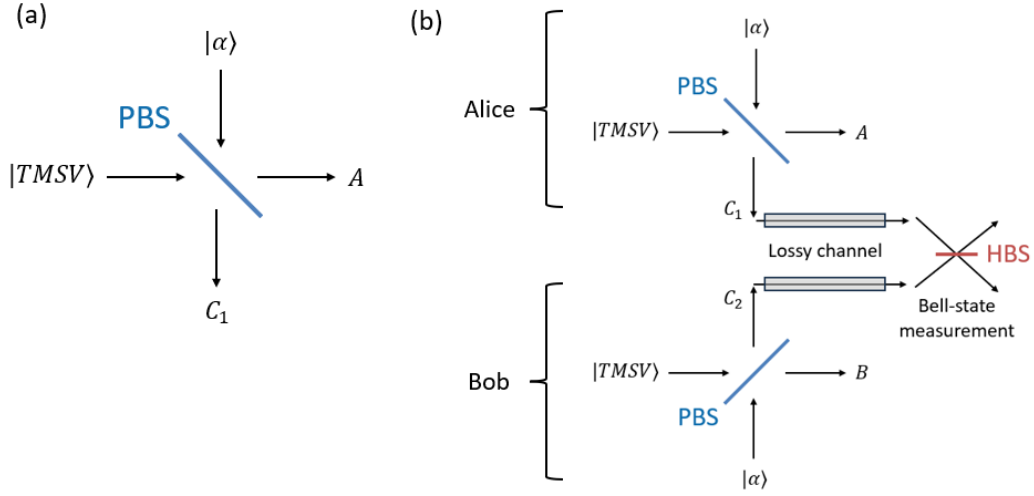


FIG. S1: Schematic of the experiment. (a) Hybrid entanglement generation. (b) Entanglement swapping.

locally by each user, where the second and third terms correspond to the hybrid entanglement,

$$\frac{1}{\sqrt{\mathcal{N}}} (\alpha |V0\rangle + \gamma |H1\rangle). \quad (4)$$

While the mode labels in Eq. (3) correspond to Alice's system, Bob prepares an identical state in modes B and C_2 . Each user transmits their photon-number qubit (mode C_1 and C_2) to the swapping node via lossy channels. At the swapping node, modes $C_1 C_2$ are projected to $|\Psi_{01}^+\rangle_{C_1 C_2} = \frac{1}{\sqrt{2}} (|10\rangle_{C_1 C_2} + |01\rangle_{C_1 C_2})$. Due to the loss during transmission, the initial state $|\psi\rangle_{AC_1} \otimes |\psi\rangle_{BC_2}$ becomes mixed. Since only specific components contribute to the projection measurement, we focus exclusively on them in what follows. Since only vertically polarized photons exist, we omit the polarization subscripts of mode C_1 and C_2 hereafter. Successful projection onto $|\Psi_{01}^+\rangle_{C_1 C_2}$ is heralded by the detection of a single photon at either output port after interfering modes C_1 and C_2 on a fiber beam splitter. Among

the terms in $|\psi\rangle_{AC_1} \otimes |\psi\rangle_{BC_2}$ that can lead to this event, the desired one are given by $\alpha\gamma|1_V0_H\rangle_A|0_V1_H\rangle_B|01\rangle_{C_1C_2}$ and $\alpha\gamma|0_V1_H\rangle_A|1_V0_H\rangle_B|10\rangle_{C_1C_2}$, with the success probability of the single-photon transmission $\sqrt{\eta_C}$. Thus, the heralding probability from ideal terms is,

$$P_{\text{ideal}} = \sqrt{\eta_C}|\alpha|^2|\gamma|^2. \quad (5)$$

On the other hand, while multiple undesired terms exist, the dominant contribution is expected from,

$$\begin{aligned} & \frac{\alpha^2\gamma}{\sqrt{2}}(|2_V0_H\rangle_A|0_V1_H\rangle_B|01\rangle_{C_1C_2} + |0_V1_H\rangle_A|2_V0_H\rangle_B|10\rangle_{C_1C_2}), \\ & \alpha^2\gamma(|1_V1_H\rangle_A|1_V0_H\rangle_B|10\rangle_{C_1C_2} + |1_V0_H\rangle_A|1_V1_H\rangle_B|01\rangle_{C_1C_2}), \\ & \gamma^2|0_V1_H\rangle_A|0_V1_H\rangle_B|11\rangle_{C_1C_2}. \end{aligned} \quad (6)$$

These terms contribute to the heralding with the following probability,

$$P_{\text{noise}} = \sqrt{\eta_C}\left[\frac{3}{2}|\alpha|^4|\gamma|^2 + (1 - \sqrt{\eta_C})|\gamma|^4\right]. \quad (7)$$

Assuming that we do not have any other imperfections, the fidelity to the ideal state $|\Psi_{\text{pol}}^+\rangle = \frac{1}{\sqrt{2}}(|HV\rangle + |VH\rangle)$ is,

$$F = \frac{P_{\text{ideal}}}{P_{\text{ideal}} + P_{\text{noise}}} = \frac{1}{1 + \frac{3}{2}|\alpha|^2 + \frac{|\gamma|^2}{|\alpha|^2}}. \quad (8)$$

Note that we assume $\sqrt{\eta_C} \ll 1$. Equation (8) indicates that the following condition is necessary to achieve high fidelity.

$$|\gamma|^2 \ll |\alpha|^2 \ll 1. \quad (9)$$

Here, the fidelity is defined as $\langle\Psi^+|\rho_{AB}|\Psi^+\rangle$, and the distributed state ρ can be described as,

$$\rho_{AB} = P_{\text{ideal}}|\Psi_{\text{pol}}^+\rangle\langle\Psi_{\text{pol}}^+| + \sqrt{\eta_C}(1 - \sqrt{\eta_C})\left[\frac{|\alpha|^4|\gamma|^2}{2}|\phi_1\rangle\langle\phi_1| + |\alpha|^4|\gamma|^2|\phi_2\rangle\langle\phi_2| + |\gamma|^4|\phi_3\rangle\langle\phi_3|\right], \quad (10)$$

where,

$$\begin{aligned} |\phi_1\rangle_{AB} &= \frac{1}{\sqrt{2}}(|1_H\rangle_A|2_V\rangle_B + |2_V\rangle_A|1_H\rangle_B), \\ |\phi_2\rangle_{AB} &= \frac{1}{\sqrt{2}}(|1_H1_V\rangle_A|1_V\rangle_B + |1_V\rangle_A|1_H1_V\rangle_B), \\ |\phi_3\rangle_{AB} &= |1_V\rangle_A|1_V\rangle_B. \end{aligned} \quad (11)$$

EVALUATION OF THE HYBRID ENTANGLEMENT

To evaluate the quality of the hybrid entangled states initially prepared at Alice and Bob, we measured the mode overlap between the SPDC photon and the weak coherent light at each location. At Alice's side, we rotated HWP_A and prepared H-polarized weak coherent light written by $|\beta\rangle_{C_1} = |0_H\rangle_{C_1} + \beta|1_H\rangle_{C_1}$. Then, the whole state of Alice is,

$$\begin{aligned} |\varphi\rangle &= |\text{TMSV}\rangle_{AC_1} \otimes |\alpha_V\rangle_A \otimes |\beta_H\rangle_{C_1} \\ &= \frac{1}{\sqrt{\mathcal{N}}}(\alpha|0_H1_V\rangle_A|0_H0_V\rangle_{C_1} + \beta|0_H0_V\rangle_A|1_H0_V\rangle_{C_1} + \gamma|1_H0_V\rangle_A|0_H1_V\rangle_{C_1} + \\ & \quad \alpha\beta|0_H1_V\rangle_A|1_H0_V\rangle_{C_1} + \gamma\alpha|1_H1_V\rangle_A|0_H1_V\rangle_{C_1} + \gamma\beta|1_H0_V\rangle_A|1_H1_V\rangle_{C_1} + \dots). \end{aligned} \quad (12)$$

Using the HWP and the PBS in *A* and *C*₁, we projected both modes to the diagonally polarized states and measured the coincidence counts between *A* and *C*₁. The coincidence probability can be calculated from,

$$P_{\text{c.c.}} = \|\langle 1_D1_D|\varphi\rangle_{AC_1}\|^2 = \left|\frac{1}{2}\gamma + \frac{1}{2}\alpha\beta + \text{others}\right|^2. \quad (13)$$

Assuming that α, β , and γ are sufficiently small that the contribution from “others” in Eq. (13) is negligible, $P_{c.c.}$ depends on the phase θ as follows,

$$P_{c.c.} = \frac{1}{4}(|\gamma|^2 + |\alpha|^2|\beta|^2 + 2|\gamma||\alpha||\beta|\cos\theta) \equiv P_\theta, \quad (14)$$

where $\theta = \varphi_\gamma - \varphi_\alpha - \varphi_\beta$ ($\varphi_\gamma, \varphi_\alpha, \varphi_\beta$ are the phase of γ, α and β). By satisfying the condition $|\alpha||\beta| = |\gamma|$, the coincidence probability exhibits full oscillation from 0 to 1 depending on the phase, under perfect mode matching between the SPDC photons and the weak coherent lights. Assuming that mode overlap probabilities in modes A and C_1 are identical and denoted by M , the coincidence probability between these modes is given by $P_\theta \propto (1 + M \cos\theta)/2$. Therefore, the oscillation visibility determined by $(P_0 - P_\pi)/(P_0 + P_\pi)$ exactly corresponds to M . This is also the case on Bob’s side.

In practice, it is difficult to completely eliminate the coincidence contributions from the “others” in Eq. (14). Therefore, we estimated the dominant contributions, $\gamma\alpha|1_H1_V\rangle_A|0_H1_V\rangle_{C_1}$ and $\gamma\beta|1_H0_V\rangle_A|1_H1_V\rangle_{C_1}$, by performing projective measurements onto $|1_V\rangle_A|1_V\rangle_{C_1}$ and $|1_H\rangle_A|1_H\rangle_{C_1}$, respectively, and subtracted them from the experimental values to evaluate the actual mode overlap.

PHASE STABILIZATION OF THE FIBER CHANNEL

We describe the feedback system used to stabilize the relative phase between photons transmitted from Alice and Bob through optical fibers, up to the point where they are combined at the swapping node. The reference light for the stabilization was provided by a continuous-wave laser at 1558 nm (WSL-110, Santec). The laser was independent of the laser source (Ultrafast optical clock, Pritel) used to generate the photon pairs at 1560 nm, and was not synchronized with that laser. As shown in Fig. 2 in the main text, the reference light was split and sent to Alice and Bob, and then recombined at the FBS after transmission through optical fibers. The interferometric light from the FBS was detected by a photodiode (PD). The electrical signal from the PD was fed into an analog PID controller (SIM960, Stanford Research Systems). The feedback signal from the PID controller was then applied to a fiber stretcher (915B, Evanescent Optics Inc.).

We show the phase stabilization results in Fig. S2. The upper figure shows the interference of the reference light, and the lower one shows that of the weak coherent light whose wavelength is the same as the flying photons. Since the reference light is directly controlled, it is well stabilized. On the other hand, there remains a slow phase drift in the weak coherent light. The measurement time is at most 1 minute on each polarization setting. Thus, the drift is not critical in this experiment. Laser synchronization and/or the sample-hold technique would be helpful for future large-scale experiments.

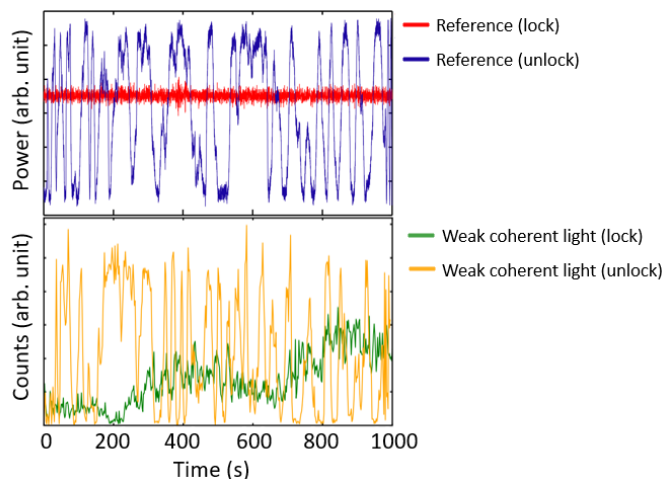


FIG. S2: Results of the phase stabilization. The upper graph shows the interference of the referential light. The lower graph shows the interference of the weak coherent light at the same wavelength as the photon-number qubit.

DISTRIBUTION OF MULTI-PARTITE ENTANGLEMENT

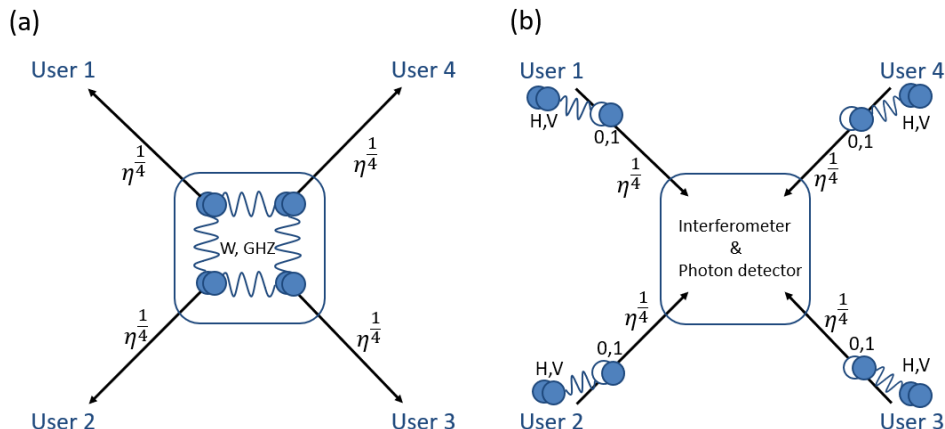


FIG. S3: Schematic image of multi-partite entanglement distribution. (a) Direct transmission protocol. (b) Protocol extending single-click entanglement swapping. All channel has the same transmittance η .

This study is compatible with a loss-tolerant protocol of multi-partite entanglement distribution proposed in Refs. [1, 2]. Here, we consider the distribution of the 4-partite polarization W- and GHZ-states in the star-type quantum network. All users are connected to the central node through channels whose transmittances are all $\eta^{1/4}$ (see Fig. S3). A conventional distribution method generates the target state at the central node and sends each photonic qubit to each end-user node. We refer to this method as "direct transmission" because it involves no repeater-like operations. In this method, all photons must survive the transmission. Thus, the distribution rate of direct transmission would scale as η .

In our protocol (combination of hybrid entanglement and Refs. [1, 2]), each user prepares a hybrid entanglement and sends a photon-number qubit to the central node. At the central node, the incoming photon-number qubits interfere with each other and are detected by single-photon detectors. Depending on the detection pattern, the quantum states remaining in the users' hands are projected accordingly: a single detector click heralds a W-state, while simultaneous clicks in two different detectors herald a GHZ-state. The local hybrid entanglement is described as follows

$$|\text{Hybrid}\rangle = \alpha |V0\rangle + \gamma |H1\rangle. \quad (15)$$

Note that we omit the normalization. The distribution of W-state The distribution rate of this protocol depends on the success probability of getting the target detection pattern and the detection probability of photons in all user nodes. In the W-state distribution, we need only one photon to be detected at the central node. One of the four users must detect photons from SPDC, while the other three must detect photons from weak coherent light. Thus, the distribution rate would be

$$R_W = |\alpha|^6 |\gamma|^2 \times \eta^{\frac{1}{4}} \times f_{\text{rep}}. \quad (16)$$

Events in which two or more users send photons, but only one is detected due to losses, contribute to noise. To suppress such events, the probability that each user sends a photon — that is, γ/α — must be kept small. In addition, multi-photon in local qubits also contributes to noise, so α must be small as well. Therefore, as in the main text, $|\gamma|^2 \ll |\alpha|^2 \ll 1$ is also required in the context of multipartite entanglement distribution. In the GHZ-state distribution, we need two photons to be detected at the central node. Two of the four users must detect photons from SPDC, while the other two must detect photons from weak coherent light. Thus, the distribution rate would be

$$R_{\text{GHZ}} \propto |\alpha|^4 |\gamma|^4 \times \eta^{\frac{1}{2}} \times f_{\text{rep}}. \quad (17)$$

We use " \propto " because the projective measurement to GHZ-state is probabilistic in Ref. [2]. The GHZ-state distribution has the same type of noise as the W-state distribution. Thus, $|\gamma|^2 \ll |\alpha|^2 \ll 1$ must be kept. In addition, a distinctive type of noise arises due to the necessity of detecting multiple photons at the central node. This noise originates from the indistinguishability between an undesirable event, in which two photons are sent from a single user, and a desirable

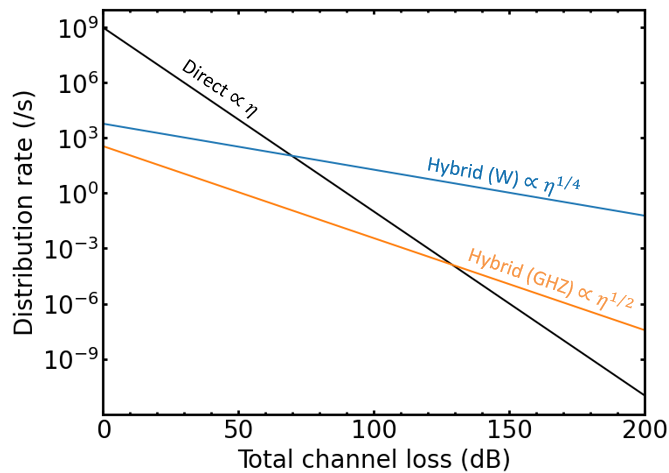


FIG. S4: Rate-loss scaling of 4-partite entanglement distribution. Direct transmission requires all four photons to survive, and thus, the rate scales as η .

event, in which one photon is sent from each of two users. In the case where two-mode squeezed vacuum (TMSV) states are used as local entanglement resources, these two types of events occur with equal probability. Reference [2] addressed this issue by spatially separating the heralded single photon into two modes. In contrast, when using hybrid entanglement as the local entanglement, the probability of the former event is inherently suppressed compared to the latter, and thus, no additional operations are required to mitigate this effect.

As we defined in the simulation of Fig. 5 in the main text, we assume $|\alpha|^2 = 0.1$, $|\gamma|^2 = 6.0 \times 10^{-3}$, $|\gamma_{\text{SPDC}}|^2 = 0.1$, and $f_{\text{rep}} = 1.0 \times 10^9$. We plot $f_{\text{rep}}\eta$, Eq. (16) and (17) with these parameters in Fig. S4. Note that we do not consider any imperfections. From Fig. S4, it is obvious that our protocol has a great advantage in rate-loss scaling.

* shimihika2357@keio.jp

† ikuta.rikizo.es@osaka-u.ac.jp

‡ takeoka@elec.keio.ac.jp

- [1] W. Roga, R. Ikuta, T. Horikiri, and M. Takeoka, Efficient Dicke-state distribution in a network of lossy channels, Phys. Rev. A **108**, 012612 (2023).
- [2] H. Shimizu, W. Roga, D. Elkouss, and M. Takeoka, Simple loss-tolerant protocol for Greenberger-Horne-Zeilinger-state distribution in a quantum network, Phys. Rev. A **111**, 022624 (2025).